BIBLIOGRAPHIC INFORMATION SYSTEM

JOURNAL FULL TITLE: Journal of Biomedical Research & Environmental Sciences
ABBREVIATION (NLM): J Biomed Res Environ Sci **ISSN:** 2766-2276 **WEBSITE:** https://www.jelsciences.com

SCOPE & COVERAGE

- **Sections Covered:** 34 specialized sections spanning 143 topics across Medicine, Biology, Environmental Sciences, and General Science
- Ensures broad interdisciplinary visibility for high-impact research.

PUBLICATION FEATURES

- **Review Process:** Double-blind peer review ensuring transparency and quality
- **Time to Publication:** Rapid 21-day review-to-publication cycle
- **Frequency:** Published monthly
- **Plagiarism Screening:** All submissions checked with iThenticate

INDEXING & RECOGNITION

- **Indexed in:** Google Scholar, IndexCopernicus (**ICV 2022: 88.03**)
- **DOI:** Registered with CrossRef (**10.37871**) for long-term discoverability
- **Visibility:** Articles accessible worldwide across universities, research institutions, and libraries

OPEN ACCESS POLICY

- Fully Open Access journal under Creative Commons Attribution 4.0 License (CC BY 4.0)
- Free, unrestricted access to all articles globally

GLOBAL ENGAGEMENT

- **Research Reach:** Welcomes contributions worldwide
- **Managing Entity:** SciRes Literature LLC, USA
- **Language of Publication:** English

SUBMISSION DETAILS

- Manuscripts in Word (.doc/.docx) format accepted

SUBMISSION OPTIONS

- **Online:** https://www.jelsciences.com/submit-your-paper.php
- **Email:** support@jelsciences.com, support@jbresonline.com

HOME ABOUT ARCHIVE SUBMIT MANUSCRIPT APC

Vision: The Journal of Biomedical Research & Environmental Sciences (JBRES) is dedicated to advancing science and technology by providing a global platform for innovation, knowledge exchange, and collaboration. Our vision is to empower researchers and scientists worldwide, offering equal opportunities to share ideas, expand careers, and contribute to discoveries that shape a healthier, sustainable future for humanity.

JOURNAL OF BIOMEDICAL RESEARCH & ENVIRONMENTAL SCIENCES
ISSN: 2766-2276
SUBJECT AREA(S): DEPRESSION | PSYCHIATRY
DOI: 10.37871

RESEARCH ARTICLE

Therapeutic Effect and Mechanism of Maizhuni-Nujia, a Classic Uyghur Prescription on Reserpine-Induced Depression in Mice

Gvlzapar Tohniyaz[1,2], Wei Chen[1,2], Zhe Xu[1,2], Yanchuan Gong[1,2] and Qin Ma[1,2*]

[1]Xinjiang Corps Key Laboratory of Bone Health and Traditional Chinese Medicine Research, Urumqi 841100, China

[2]Xinjiang Huashidan Pharmaceutical Research Co., Ltd., Urumqi 841100, China

Abstract

Introduction: Major depressive disorder is a prevalent psychiatric condition affecting millions worldwide, yet current pharmacotherapies, primarily based on monoamine modulation, are limited by delayed onset, insufficient efficacy, and adverse effects. Maizhuni-Nujia (MZNNJ) is a classic multi-herb prescription from Uyghur traditional medicine, traditionally used for melancholia and amnesia, but its antidepressant mechanisms and scientific basis remain largely unexplored. This study aimed to systematically investigate the antidepressant effects and underlying mechanisms of MZNNJ using a reserpine-induced acute depression model in mice.

Methods: An acute depression model was established in mice by intraperitoneal injection of reserpine (4 mg/kg). Mice were pre-treated orally with various doses of MZNNJ (6.15, 12.3, or 24.6 g/kg), its individual herbal components (processed or unprocessed), or fluoxetine (4.1 mg/kg) for 14 days. Behavioral assessments included eyelid ptosis, the circle escape test, and the Morris water maze. Neurochemical markers (5-HT, DA, BDNF) were measured by ELISA, and histopathological changes in the hippocampus and cortex were evaluated with H&E staining. Proteomic and metabolomic profiling of brain tissue were performed using DIA-based mass spectrometry and UHPLC-MS/MS, respectively. Key proteins in the Ras/ERK/CREB/BDNF signaling pathway were validated by Western blotting and immunofluorescence.

Results: MZNNJ treatment dose-dependently ameliorated reserpine-induced depressive-like behaviors, including ptosis, reduced escape behavior, and spatial learning and memory deficits. This was accompanied by significant restoration of 5-HT, DA, and BDNF levels in both serum and brain tissue, and marked improvement in neuronal damage in hippocampal subregions. Comparative analysis revealed that the formulation containing processed

***Corresponding author(s)**

Qin Ma, Xinjiang Corps Key Laboratory of Bone Health and Traditional Chinese Medicine Research, Urumqi 841100, China
Email: mq7895@163.com
DOI: 10.37871/jbres2317

Submitted: 20 July 2026

Accepted: 27 July 2026

Published: 28 July 2026

Keywords

- Maizhuni-Nujia
- *Reserpine-induced depression*
- KSR1
- Ras/ERK/CREB/BDNF
- Neuroplasticity

How to cite this article: TohniyazG, ChenW, Xu Z, Gong Y, Ma Q. Therapeutic Effect and Mechanism of Maizhuni-Nujia, a Classic Uyghur Prescription on Reserpine-Induced Depression in Mice. J Biomed Res Environ Sci. 2026 July 28; 7(7): 25. Doi: 10.37872/jbres2317

herbs (ACFI and MPF) was significantly more efficacious than the formulation containing raw herbs. Proteomics and subsequent validation showed that MZNNJ robustly reversed the reserpine-induced downregulation of KSR1, Ras, p-ERK, p-CREB, and BDNF. Metabolomics further revealed that MZNNJ corrected brain metabolic disturbances, with significant enrichment in pathways related to glutathione metabolism, energy metabolism, and the "Spinocerebellar ataxia" pathway.

Conclusion: This study provides the first comprehensive evidence that MZNNJ exerts potent antidepressant effects through multifaceted mechanisms involving activation of the KSR1-mediated Ras/ERK/CREB/BDNF neurotrophic pathway and systemic restoration of brain metabolic homeostasis. These findings validate the traditional processing and compatibility principles of Uyghur medicine and position MZNNJ as a promising candidate for further development as a novel antidepressant therapy.

Graphical Abstract

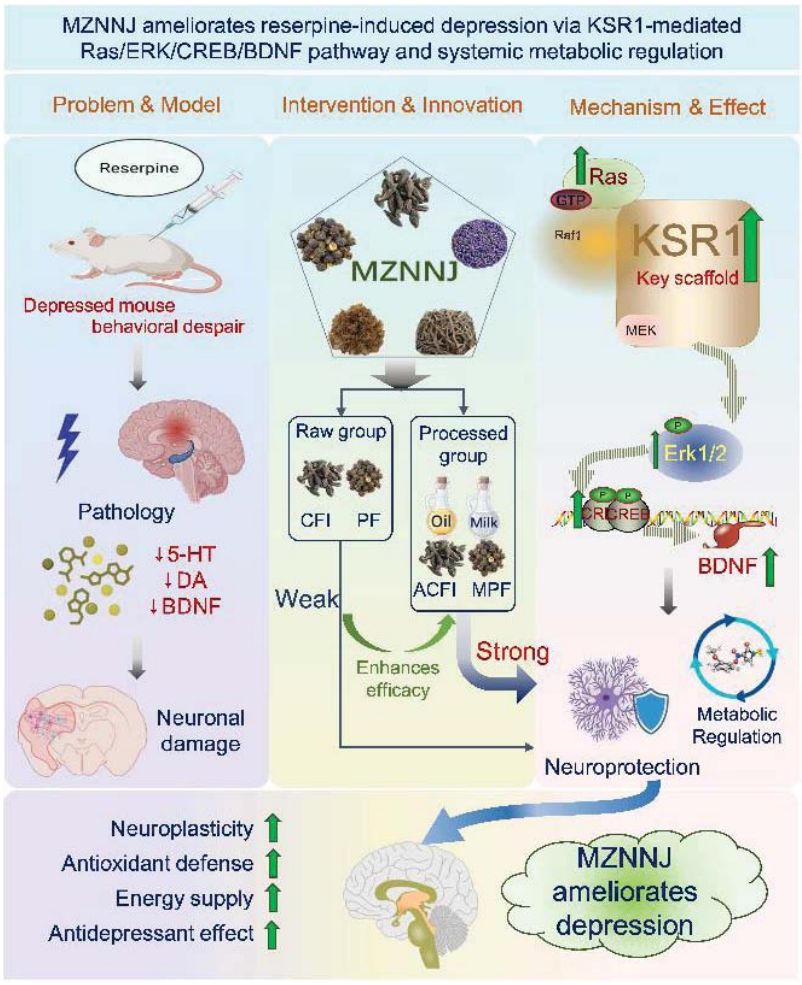

Introduction

Major Depressive Disorder (MDD) is a prevalent and debilitating psychiatric condition characterized by persistent low mood, anhedonia, cognitive dysfunction, and neurovegetative disturbances [1,2]. With a global prevalence affecting over 350 million people, MDD is a leading cause of disability worldwide and is projected to become the second largest contributor to the global disease burden [3,4]. While current first-

line pharmacological treatments, primarily based on the monoamine hypothesis, offer therapeutic benefits, they are often associated with significant limitations, including delayed onset of action, limited efficacy, and a range of adverse effects that impact patient compliance [5,6]. This has spurred an ongoing search for novel, more effective, and safer therapeutic agents, with a growing interest in exploring the rich pharmacopeia of traditional medicine systems [7,8].

Maizhuni-Nujia (MZNNJ) is a classic compound prescription from the Uyghur system of traditional medicine, documented in the ancient text "Bai Di Yi Yao Shu" (1368 AD). It is traditionally indicated for conditions resembling melancholia and amnesia. The prescription is composed of five medicinal herbs: Chebulae Fructus Immaturus (CFI, immature fruit of *Terminalia chebula* Retz.), Phyllanthi Fructus (PF, fruit of *Phyllanthus emblica* L.), *Cuscuta chinensis* Lam. (seed), *Lavandula angustifolia* Mill. (Aerial parts), and *Polypodiode snipponica* (Mett.) Ching (rhizome). In clinical practice, specific traditional processing methods are applied to the two sovereign herbs, CFI and PF, before they are combined into the final formula. CFI is processed by stir-frying with apricot kernel oil (to produce ACFI, almond oil-processed Chebulae Fructus Immaturus), and PF is processed by soaking in raw milk (to produce MPF, milk-processed Phyllanthi Fructus). These processing techniques are believed to enhance efficacy and reduce potential toxicity, a core tenet of many ethnomedical systems [9,10]. Despite its historical use, the antidepressant effects and underlying mechanisms of MZNNJ have not been systematically investigated using modern scientific approaches.

The reserpine-induced depression model is a well-established pharmacological model for screening antidepressant activity [11,12]. Reserpine irreversibly inhibits the Vesicular Monoamine Transporter 2 (VMAT2), leading to the depletion of monoamine neurotransmitters such as serotonin (5-HT), Dopamine (DA), and Norepinephrine (NE) from synaptic vesicles in the central and peripheral nervous systems [13,14]. This depletion reliably induces a spectrum of behavioral and physiological changes in rodents that mirror key aspects of depression, including ptosis, hypolocomotion, and anhedonia, making it a valuable tool for studying monoamine-related pathophysiology and evaluating potential antidepressant interventions [15].

In this study, we employed the reserpine-induced mouse model of depression to comprehensively evaluate the antidepressant efficacy of MZNNJ. Using a multi-faceted approach integrating behavioral, neurochemical, histopathological, proteomic, and metabolomic analyses, we aimed to (1) confirm the antidepressant effects of MZNNJ, (2) dissect the contribution of its constituent herbs and their traditional processing, and (3) elucidate its underlying molecular mechanisms, with a particular focus on key signaling pathways and metabolic networks implicated in depression.

Materials

Animals

A total of 110 KM mice (7 weeks old, weighing 18 ± 2g) were provided by Animal Center, Xinjiang Medical University (Urumqi, China, Certificate No. SCXK (XING) 2024-0001). The rooms had a 12 h light/dark cycle, constant temperature and humidity, and free access to standard laboratory food and water. Animal studies were carried out under the Guiding Principles for the Care and Use of Laboratory Animals. The feeding and environmental conditions were established by the regulations of the Animal Ethics Committee of Xinjiang Corps Key Laboratory of Bone Health and Traditional Chinese Medicine Research (Approval number: HSD-20241110-04).

Drugs and chemicals

Maizhuni-Nujia (MZNNJ, Huashidan, China), Xiqingguo (*Chebulae Fructus Immaturus*, CFI, Sichuan Province, China), Almond oil processed-Chebulae Fructus Immaturus (ACFI, Huashidan, China), Yuganzi (*Phyllanthi Fructus*, PF, Guizhou, China), Milk processed-Phyllanthi Fructus (MPF, Huashidan, China), Fluoxetine Hydrochloride Capsules (Huairen, China), Reserpine Injection (Jinyao, China), Mouse 5-Hydroxytryptamine/serotonin Elisa Kit, Dopamine Elisa Kit, Mouse Brain Derived Neurotrophic Factor Elisa Kit (Thermo Fisher, USA), BCA Protein Quantification Kit, Anti-KSR1 Rabbit pAb, Anti-Ras Rabbit pAb, Anti-CREB Rabbit pAb, Anti-Phospho-CREB (S133) Rabbit pAb, Anti-ERK1+ERK2 Rabbit pAb, Anti-Phospho-ERK1 (T202/Y204) + ERK2 (T185/Y187) Rabbit pAb, Anti-BDNF Rabbit pAb, Prestained Protein Marker, Ultra-sensitive ECL chemiluminescence kit (Servicebio, China), HRP-labeled goat anti-rabbit IgG antibody (Boster, China).

Experimental instruments

IVC Animal Experiment System (FENGSHI Group, China), Morris Water maze (Zhenghua Biology, China), Microplate Readers (Molecular Devices, USA), Western-blot system (Bio-Rad, USA).

Methods

Pharmaceutical preparation

ACFI preparation: Place the Almond oil in a roasting machine and preheat it (heat until the oil temperature reaches 130˚C as measured by a thermometer). Add the cleaned Xingqing fruit (with a ratio of CFI to Almond oil of 1:0.3) to the stir-frying machine. Continuously stir-fry at 20 rpm for 10 minutes. Remove and drain the oil until no oil droplets fall, and the product is ready.

MPF preparation: Take the PF, remove the seeds, remove any impurities, wash thoroughly, and dry. Add raw milk at a ratio of 1:15 (g/mL) to the fruit, stir well, and soak at room temperature for 16 hours. Remove, rinse to remove excess milk residue, and dry at low temperature, and the product is ready.

MZNNJ preparation: Take the powdered forms of ACFI, MPF, Rhizoma Polypodii (RP, the rhizome of Polypodiode snipponica), Herba Cuscutae (HC, the seed of Cuscuta chinensis Lam.), and Herba Lavandulae (HL, the aerial parts of Lavandula angustifolia Mill.). Mix them in a ratio of ACFI:MPF:RP:HC:HL= 5:5:1:1:1. Mix the herbal powder with honey at a temperature below 60°C in a 1:3 ratio and stir thoroughly until evenly combined. The final product is obtained.

Preparation of MZNNJ suspention and UPLC-Q Exactive-orbitrap-MS analysis

Take a 200 mg sample of MZNNJ herbal powder, add 50% methanol-water solution (v/v, methanol: water = 50:50), sonicated for 30 minutes, and 1 mL of the supernatant was transferred to a centrifuge tube. The tube was centrifuged at 14,000 rpm for 5 minutes, and the supernatant was filtered through a 0.22 μm microporous membrane before being transferred to a sample vial for UHPLC-MS/MS analysis. Blank samples were processed under the same conditions.

The separation was performed using an ACQUITY UPLC HSS T3 Column (2.1×100 mm, 1.8 μm) at a temperature of 35˚C and a flow rate of 0.3 mL/min. The optimal mobile phases consisted of 0.1: 100 (v/v) HCOOH/H_2O (solvent A) and 0.1:100 (v/v) HCOOH/acetonitrile (solvent B). The optimized UPLC elution conditions were as follows: 0 to 10 min, 0 to 30% B; 10 to 25 min, 30 to 40% B; 25 to 30 min, 40 to 50% B; 30 to 40 min, 50 to 70% B; 40 to 45 min, 70 to 100% B; 45 to 60 min, 100% B; 60 to 70 min, 100% A. The injection volume was set at 10 μL. The mass spectrum data was acquired in both positive and negative ion mode through Full MS-ddMS2

mode by the Q Exactive Orbitrap high resolution mass spectrometer. The scan parameters were set as follows: scan range, 100 to 1200 m/z; MS^1 resolution, 70000; MS^2 resolution, 17500; ion source voltage, 3.2kV; capillary temperature, 320°C; auxiliary gas heater temperature, 350°C; Sheath gas flow rate, 40 L/min; AGC target, 1×10^6; TopN, 5. The Normalized Collision Energy (NCE) was set at 30, 40, and 50 V.

Mouse grouping and drug administration

Mice were randomly divided into 11 groups based on body weight, Wild Type group (WT): distilled water; Model group (Mod): distilled water; Fluoxetine group (FXT): 4.1 mg/kg fluoxetine aqueous solution; CFI group: 0.6g/kg CFI powder aqueous solution; ACFI group: 0.6g/kg ACFI powder aqueous solution; PF group: 0.6g/kg PF powder aqueous solution; MPF group: 0.6g/kg MPF powder aqueous solution; Raw MZNNJ group (Raw): 6.15g/kg MZNNJ aqueous solution containing CFI and PF; MZNNJ low dose group (Low): 6.15g/kg MZNNJ aqueous solution containing ACFI and MPF; MZNNJ middle dose group (Mid): 12.3g/kg MZNNJ aqueous solution containing ACFI and MPF; MZNNJ High dose group (Hig): 24.6g/kg MZNNJ aqueous solution containing ACFI and MPF. with 10 mice in each group and equal numbers of males and females (males and females were housed separately). After 7 days of adaptation, the mice were administered the drug via gavage for 14 days, with daily measurements of body weight

Model establishment and behavioral testing

24hours after the last dose, the experimental group was administered reserpine via intraperitoneal injection at a concentration of 4 mg/kg, while the WT group received an equal volume of saline solution. Half an hour after reserpine administration, the animals were observed for eyelid drooping, followed by behavioral testing (Morris Water maze). The circle escape rate was measured approximately four hours after reserpine administration.

Criteria for determining the degree of eyelid ptosis: fully open 0 degrees; 1/4 ptosis 1 degree; 1/2 ptosis 2 degrees; 3/4 ptosis 3 degrees; fully closed 4 degrees. Morris Water maze: Prepare a circular water tank with a diameter of approximately 120 cm and a water depth of about 30 cm for the mouse water maze. In the center of the tank, install a platform that can be submerged underwater, with a height that allows the animal to stand on it and remain above the water surface. Additionally, install cameras and other tracking systems to record the animal's movement trajectories within the water maze, and use appropriate tracking software for data analysis; maintain the laboratory environment under constant temperature and lighting conditions, with room and water temperatures typically around 22°C. Lighting should be as dim as possible to reduce animal stress and platform visibility, while ensuring sufficient illumination for detection via the tracking software (pre-training, localization training, and position detection training are performed prior to detection. All training is conducted before the injection of reserpine for modeling) [16,17]; position detection test, same as position detection training, record the time taken to find the platform within 90 seconds. If not found, record the time spent and number of crossings in the target quadrant within 90 seconds. Escape rate: Observe each mouse for 15s within a white paper circle with a diameter of 7.5 cm to see if it exits the circle, record the number of exits, and calculate the circle escape rate for each group of animals.

Detection of 5-HT, DA, and BDNF levels

The levels of 5-HT, DA, and BDNF in the serum and brain homogenate of mice with acute depression induced by reserpine were detected using the Enzyme-Linked Immunosorbent Assay (ELISA). Blood was collected from the orbital cavity of mice, stand at room temperature for 2 hours, then centrifuged at 4°C and 3000 rpm for 10 minutes. The precipitate was discarded, and

the supernatant serum was reserved for later use. After euthanizing the mice, quickly remove the brain tissue, wash off the surface blood with pre-chilled PBS, and grind the tissue in an ice bath at a tissue-to-PBS volume ratio of 1:9. Centrifuge at 4˚C at 12000g for 15 minutes, then collect the supernatant for later use. Follow the instructions in the ELISA kit manual for testing.

Histopathological analysis

After euthanizing the mice, the brain tissue was quickly removed and preserved in 4% formaldehyde fixative. The fixed brain tissue was dehydrated with ethanol, permeated with xylene, and immersed in liquid paraffin. After paraffin penetration, the tissue was cooled, sectioned into 6μm thick slices, mounted on slides, and dried. Subsequently, dewaxing was performed using xylene, followed by rehydration with a series of ethanol solutions ranging from high to low concentrations, and finally immersed in distilled water. The sections were then stained with hematoxylin-eosin. The stained sections are dehydrated using a series of ethanol solutions ranging from low to high concentrations, followed by xylene clarification. They are then coated with neutral resin, covered with a glass cover slip, and observed under a microscope.

Data independent acquisition quantitative proteomics analysis

2.8. Take mouse brain tissue, grind it with liquid nitrogen, add an appropriate amount of SDT lysis buffer, transfer it to an EP tube, then boil it in a water bath for 3 minutes, sonicate it for 2 minutes, centrifuge it at 4˚C at 16,000g for 20 minutes, take the supernatant, and use the BCA method to quantify the protein. For each sample, an appropriate amount of protein was subjected to FASP enzymatic digestion. The digested peptides were dried and redissolved in 0.1% formic acid. The peptide concentration was measured for LC-MS analysis. Chromatographic separation was performed using the Vanquish Neo UHPLC system. After separation, the peptides were analyzed by DIA (data-independent acquisition) mass spectrometry using the Orbitrap Astral mass spectrometer. All mass spectrometry data were merged using the DIA-NN software to complete database searching and protein DIA quantification analysis. The database used was uniprotkb-Mus musculus (Mouse) [10090]-87491-20241204.fasta, obtained from the website https://www.uniprot.org/taxonomy/10090, downloaded on 20241204.

Western blot analysis

Take mouse brain tissue, grind it with liquid nitrogen, add an appropriate amount of RIPA lysis buffer, transfer it to an EP tube, lyse it on ice for 30 minutes at 4˚C, centrifuge at 12,000g for 15 minutes, take the supernatant, and quantify the protein using the BCA method. Mix each group of protein samples with 5× sample buffer at a ratio of 4:1 and boil at high temperature for 10 minutes. All protein samples were separated using 10% SDS-PAGE, then transferred to a PVDF membrane. The membrane was blocked with a protein-free rapid blocking solution for 30 minutes, followed by incubation with the corresponding primary antibody overnight at 4˚C. The membrane was then incubated with the secondary antibody at room temperature for 2 hours. The membrane was washed three times with TBST, each for 10 minutes. Protein bands were visualized using ECL fluorescent reagents on an imaging system.

Immunofluorescence analysis

Place brain tissue in 4% paraformaldehyde for fixation, dehydrate in sucrose, and then freeze-section. Permeabilize with TritonX-100, followed by incubation at room temperature for 30 minutes. Block with 10% bovine serum at room temperature for 30 minutes. Prepare the primary antibody p-CREB and incubate overnight at 4˚C. Add the fluorescent secondary antibody and incubate at room temperature

in the dark. Add DAPI staining solution and incubate at room temperature in the dark for 5 minutes, then mount with an anti-fade agent. Finally, image the mounted slides using a fluorescence microscope.

Metabolomics analysis

Thaw serum frozen at -80˚C at 4˚C, vortex to mix, transfer 100 µL to an EP tube, add 300 µL of pre-chilled methanol, mix, sonicate in an ice bath for 20 minutes, incubate at -20˚C for 1 hour, centrifuge at 16000g at 4˚C for 20 minutes. Take 50mg of brain tissue, place it in an EP tube, add 2 steel beads, add 430µL of pre-chilled methanol, homogenize and disrupt the tissue in a tissue homogenizer at low temperature, mix thoroughly, sonicate in an ice bath for 20 minutes, incubate at -20˚C for 1 hour, and centrifuge at 16000 g at 4˚C for 20 minutes. Take an appropriate amount of supernatant, place the sample in an automatic sampler at 4˚C, and analyze the sample using the SHIMADZU-LC30 UHPLC system. After UPLC separation, the sample is analyzed by mass spectrometry using a QE Plus mass spectrometer.

Raw data were processed using MSDIAL software for peak alignment, retention time correction, and peak area extraction. Metabolite structural identification was performed using exact mass matching (mass tolerance < 10ppm) and secondary spectrum matching (mass tolerance < 0.01Da), with searches conducted in public databases such as HMDB, MassBank, and GNPS. For the extracted data, ion peaks with missing values exceeding 50% within a group were excluded from subsequent statistical analysis. Positive and negative ion data were normalized by total peak area, and positive and negative ion peaks were integrated and analyzed using pattern recognition with Python software. After preprocessing with unit variance scaling (UV), the data underwent further analysis.

Statistical analysis

All experimental data are expressed as mean ± standard deviation (SD) and analyzed and plotted using GraphPad 10 statistical software. Intergroup differences were assessed using one-way analysis of variance (ANOVA). Following a significant ANOVA result, Tukey's honestly significant difference (HSD) post-hoc test was used for multiple comparisons between groups. For comparisons involving only two groups, Student's t-test (two-tailed) was applied. A $p < 0.05$ was considered statistically significant. All behavioral and biochemical assays were performed with adequate sample sizes to ensure statistical power ($n \geq 8$ per group for ELISA; $n = 3$ per group for Western blotting and proteomics).

Result

Identification of components in MZNNJ

UPLC-Q Exactive-Orbitrap-MS analysis was used to investigate the main chemical components in the MZNNJ formula. Compound Discover 3.2 software was used to extract characteristic peaks from raw mass spectrometry data, with a mass deviation of less than 5 ppm set for characteristic peak element matching, molecular formula prediction, and isotope distribution matching. Characteristic peaks were identified using the mzCloud online database and the locally built mzVault traditional Chinese medicine natural product database. Positive results were screened based on the following criteria: mass deviation < 5 ppm, consistent isotope distribution, and mzVault best match database score > 70. Mass spectrometry data were collected in both positive and negative ion modes, with the total ion chromatograms shown in figures 1 (A-B). A total of 71 compounds were identified, with the top 10 compounds by content shown in figure 1C.

Effect of MZNNJ on body weight and behavior of the mice

There were no significant changes in body weight between groups before and after 14 days of administration in 11 groups of mice (p

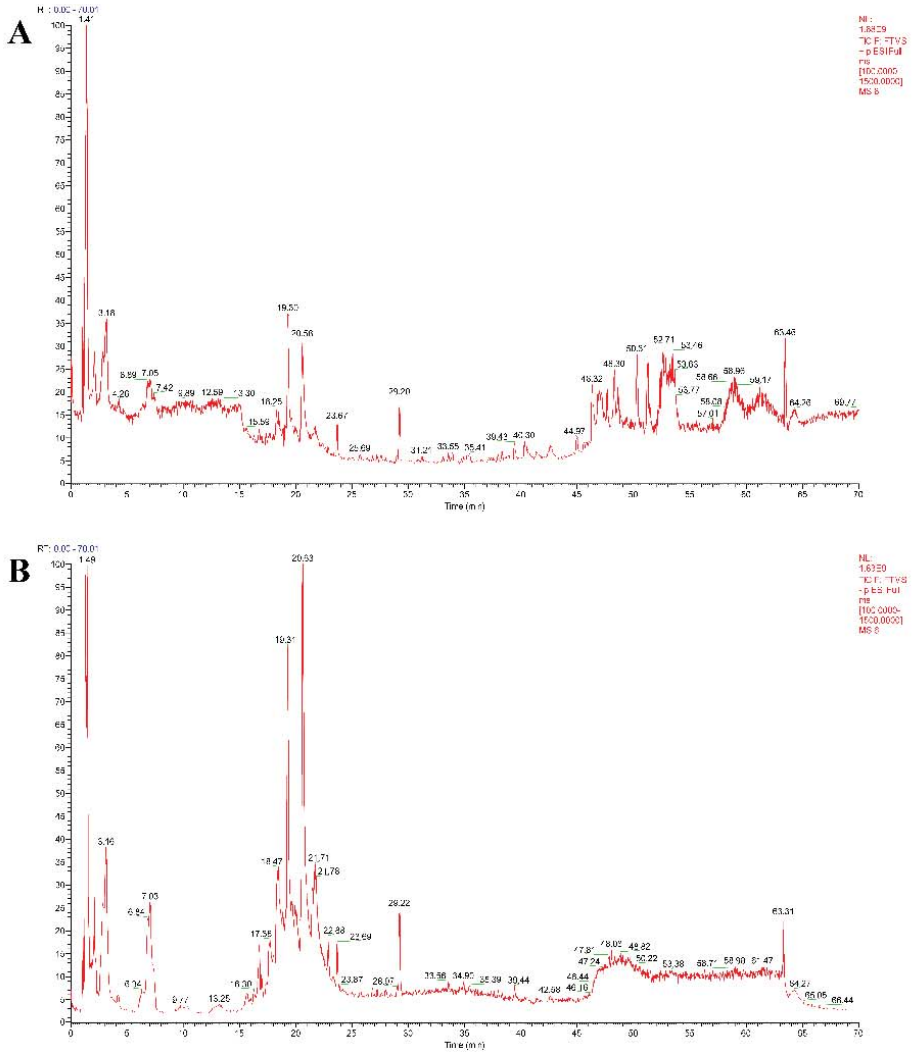

C

Compound name	Molecular formula	Retention (min)	Relative content (%)
Ellagic acid	$C_{14}H_6O_8$	21.515	26.663
Betaine	$C_5H_{11}NO_2$	1.412	16.529
Quinic acid	$C_7H_{12}O_6$	1.462	10.468
Gallic acid	$C_7H_6O_5$	6.816	6.078
Shikimic acid	$C_7H_{10}O_5$	2.101	5.624
Pyrogallol	$C_6H_6O_3$	7.046	4.363
Lactose	$C_{12}H_{22}O_{11}$	1.402	3.003
Citric acid	$C_6H_8O_7$	3.073	2.682
Sucrose	$C_{12}H_{22}O_{11}$	1.462	2.568
Rosmarinic acid	$C_{18}H_{16}O_8$	22.872	2.447

Figure 1 Total ion chromatogram of MZNNJ using UPLC-Q-Exactive-orbitrap-MS.

(A) Total ion chromatogram in positive ion mode. (B) Total ion chromatogram in negative ion mode. (C) Top 10 compounds identified by content in MZNNJ. The chemical components were identified by matching retention times, molecular masses, and MS/MS fragmentation patterns against the mzCloud and mzVault databases. n = 3 independent injections per sample.

> 0.05), shown in figure 2A. Half an hour after reserpine injection, the degree of eyelid ptosis in mice was observed. The Mod group showed a significantly higher degree of ptosis than the WT group ($p < 0.001$); the PF and MPF groups showed significantly lower degrees of ptosis

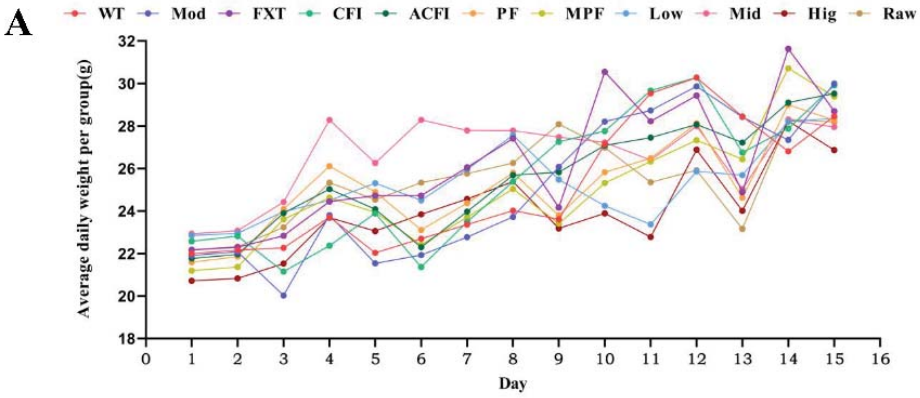

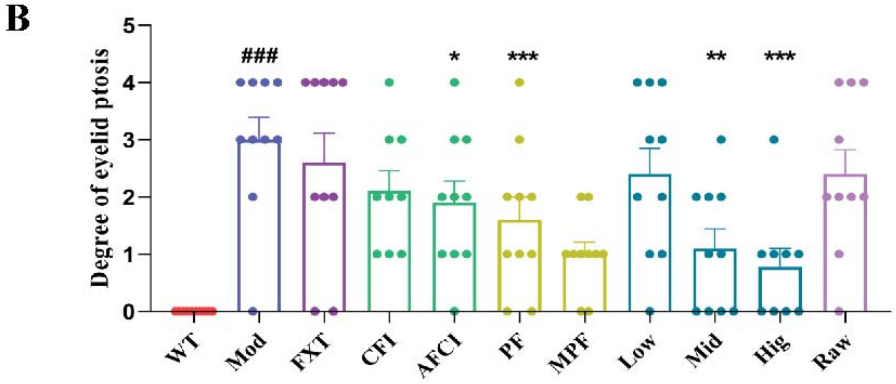

C

Group	Escape mice	Total mice	Escape rate (%)
WT	10	10	100
Mod	0	10	0
FXT	1	9	11.11
CFI	2	10	20
ACFI	2	10	20
PF	1	10	10
MPF	1	10	10
Low	3	10	30
Mid	3	10	30
Hig	6	9	66.67
Raw	5	10	50

Figure 2 MZNNJ ameliorates reserpine-induced behavioral deficits in mice.

(A) Body weight changes before and after 14 days of administration. (B) Eyelid ptosis score assessed 30 min after reserpine injection. (C) Circle escape rate measured 4 h after reserpine injection. Data are presented as mean ± SD (n = 10 per group). Statistical analysis was performed using one-way ANOVA followed by Tukey's post-hoc test for multiple comparisons. ###p < 0.001 vs. WT group; *$p < 0.05$, **$p < 0.01$, ***$p < 0.001$ vs. Model group.

than the Mod group ($p < 0.05$, $p < 0.001$); In the MZNNJ treatment group, the eyelid ptosis in the Mid and Hig groups was significantly lower than that in the model group ($p < 0.01$, $p < 0.001$), as shown in figure 2B. After injection of reserpine, the mice exhibited reduced movement and lethargy. Several mice in the drug-treated group escaped, with the highest escape rate observed in the MZNNJ Hig group, as shown in figure 2C.

The results of the Morris water maze experiment show that after injection of reserpine, mice exhibited despair, ceased swimming, and merely floated on the water surface. In contrast, the WT group swam normally, and the latency period (time taken to locate the platform) was shorter. Analysis was conducted based on latency

period, total distance traveled, average speed, and the number of mice reaching the platform. Compared to the WT group, the Mod group showed a significantly longer latency period ($p < 0.01$), significantly shorter total swimming distance ($p < 0.05$), significantly slower average speed ($p < 0.001$), and a reduced number of mice reaching the platform; the MZNNJ Low and Mid groups had significantly longer total swimming distances than the Mod group ($p < 0.05$); The average speed of the MZNNJ Low group was significantly higher than that of the Mod group ($p < 0.01$), as shown in figures 3A-E.

Effect of MZNNJ and the herbs in the formula on the levels of 5-HT, DA, and BDNF in mice with acute depression

The levels of 5-HT ($p < 0.05$), DA ($p < 0.001$), and BDNF ($p < 0.01$) in the serum of Mod group mice were significantly lower than those in the WT group. The MZNNJ treatment group showed varying degrees of increase compared

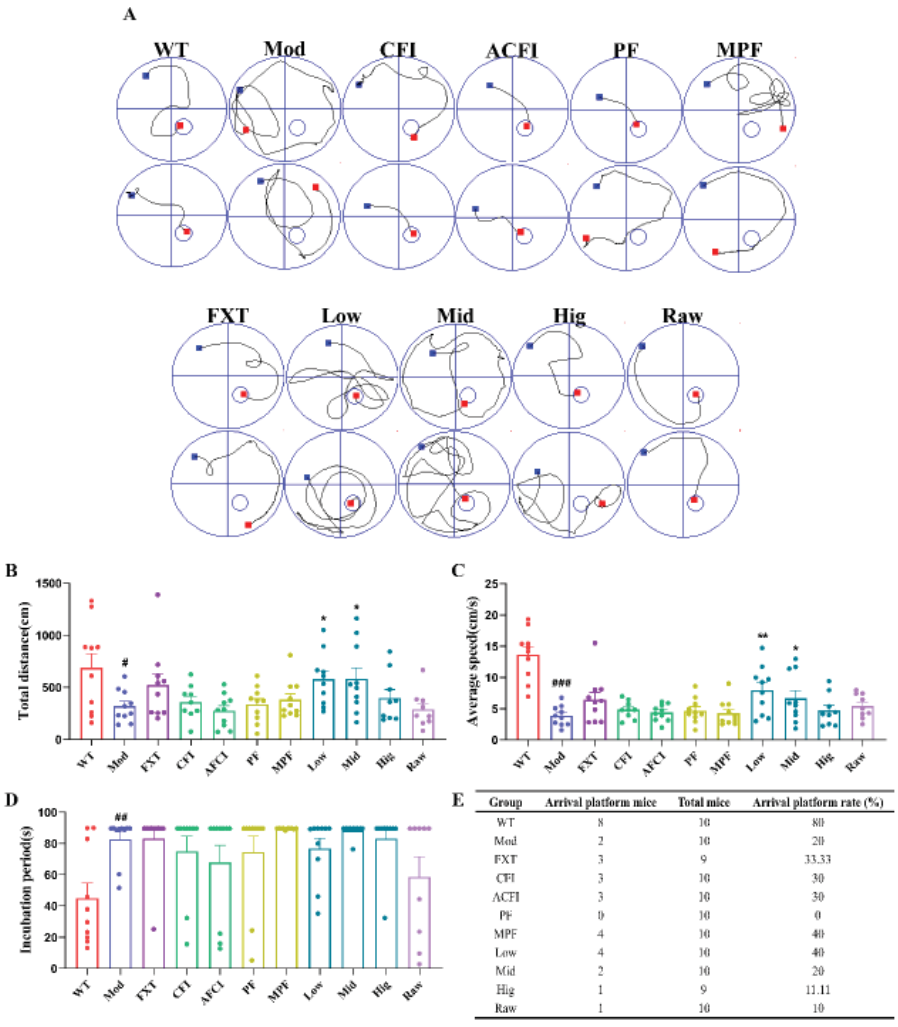

Figure 3 MZNNJ ameliorates reserpine-induced spatial learning and memory deficits in the Morris water maze test.

(A) Representative swimming trajectories of mice from each group during the probe trial. (B) Escape latency to find the hidden platform. (C) Total swimming distance. (D) Average swimming speed. (E) Number of mice reaching the platform within 90 s. Data are presented as mean ± SD (n = 10 per group). Statistical analysis was performed using one-way ANOVA followed by Tukey's post-hoc test for multiple comparisons. #$p < 0.05$, ##$p < 0.01$, ###$p < 0.001$ *vs*. WT group; *$p < 0.05$, **$p < 0.01$, vs. Model group.

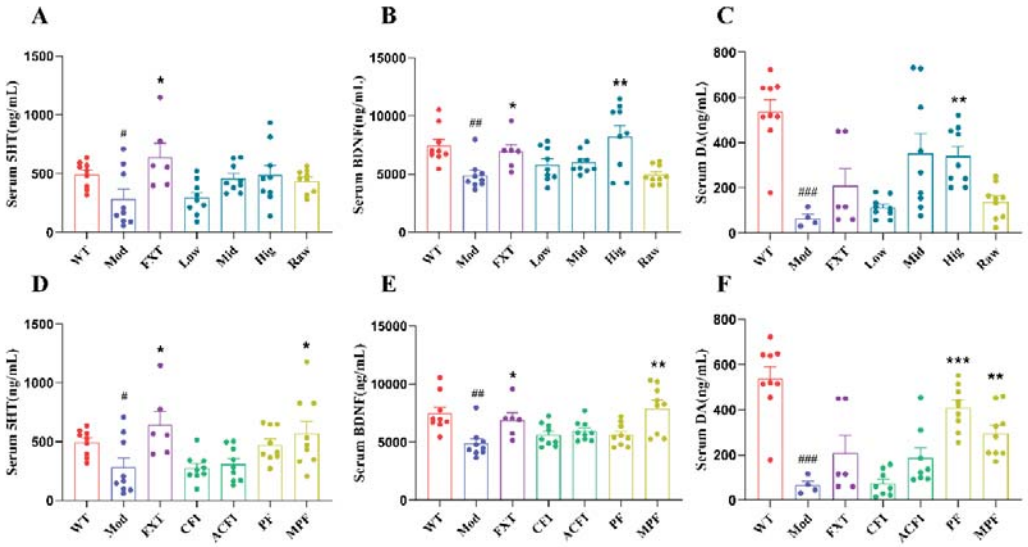

Figure 4 Effects of MZNNJ and its constituent herbs on serum levels of 5-HT, DA, and BDNF in reserpine-induced depressed mice.

(A–C) Serum concentrations of (A) 5-hydroxytryptamine (5-HT), (B) dopamine (DA), and (C) brain-derived neurotrophic factor (BDNF) in mice treated with different doses of MZNNJ. (D–F) Serum concentrations of (D) 5-HT, (E) DA, and (F) BDNF in mice treated with individual herbal components (CFI, ACFI, PF and MPF). All values were measured by ELISA. Data are presented as mean ± SD (n = 8 per group). Statistical analysis was performed using one-way ANOVA followed by Tukey's post-hoc test for multiple comparisons. ###p < 0.001 vs. WT group; *p < 0.05, **p < 0.01, ***p < 0.001 vs. Model group.

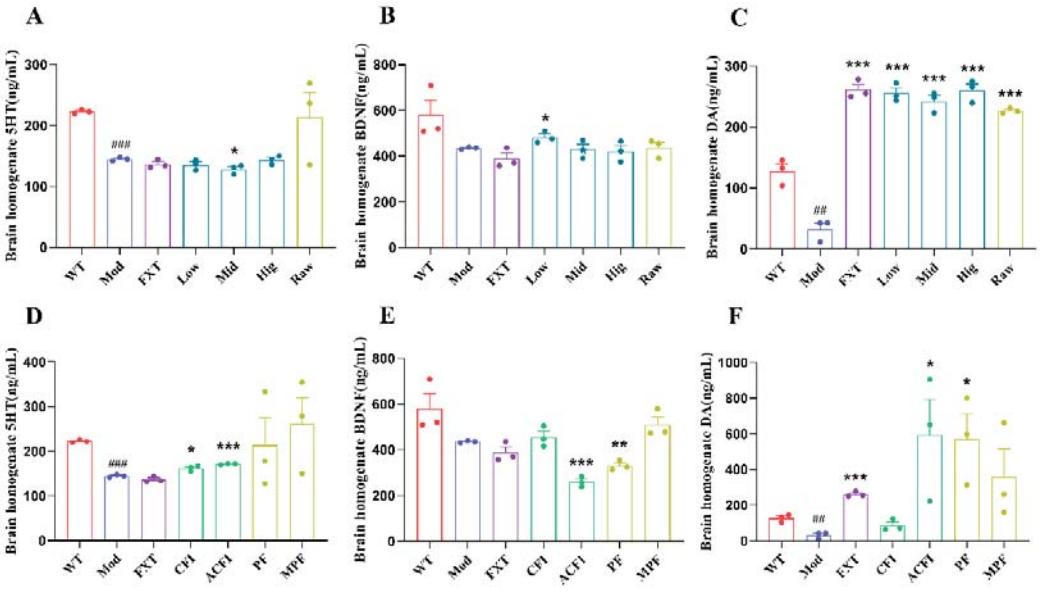

Figure 5 Effects of MZNNJ and its constituent herbs on brain tissue levels of 5-HT, DA, and BDNF in reserpine-induced depressed mice.

(A–C) Brain homogenate concentrations of (A) 5-HT, (B) DA, and (C) BDNF in mice treated with different doses of MZNNJ. (D–F) Brain homogenate concentrations of (D) 5-HT, (E) DA, and (F) BDNF in mice treated with individual herbal components (CFI, ACFI, PF, MPF). All values were measured by ELISA. Data are presented as mean ± SD (n = 8 per group). Statistical analysis was performed using one-way ANOVA followed by Tukey's post-hoc test for multiple comparisons. ###p < 0.001 vs. WT group; *p < 0.05, **p < 0.01, ***p < 0.001 vs. Model group.

to the Mod group, with significant elevations in BDNF and DA levels in the Hig group ($p < 0.01$). In the single-herb group, compared with the Mod group, the MPF group showed a significant increase in 5-HT ($p < 0.05$); the PF group ($p < 0.001$) and MPF group ($p < 0.01$) showed significant increases in DA levels; and the MPF group showed a significant increase in BDNF levels ($p < 0.01$), as shown in figures 4A-E.

The 5-HT ($p < 0.001$) and DA ($p < 0.01$) levels in brain homogenates of Mod group mice were significantly lower than those in the WT group. Compared with the Mod group, all doses of MZNNJ administration significantly increased DA levels ($p < 0.001$), and the Low dose group showed a significant increase in BDNF ($p < 0.05$). Compared to the Mod group, the monotherapy groups showed significantly increased 5-HT levels in the CFI group ($p < 0.05$) and ACFI group ($p < 0.001$). Both the ACFI and PF groups exhibited significantly elevated BDNF levels ($p < 0.01$) and DA levels ($p < 0.05$), as shown in figures 5A-E.

Effects of MZNNJ on mouse brain tissue structure

Histological sections reveal that in the Mod group, compared to the WT group, the number of cortical neurons decreased and nuclei became disorganized. In the hippocampal CA1 and CA3 regions, neuronal arrangement was disordered and nuclei were disorganized. The DG region exhibited reduced neuronal numbers, markedly

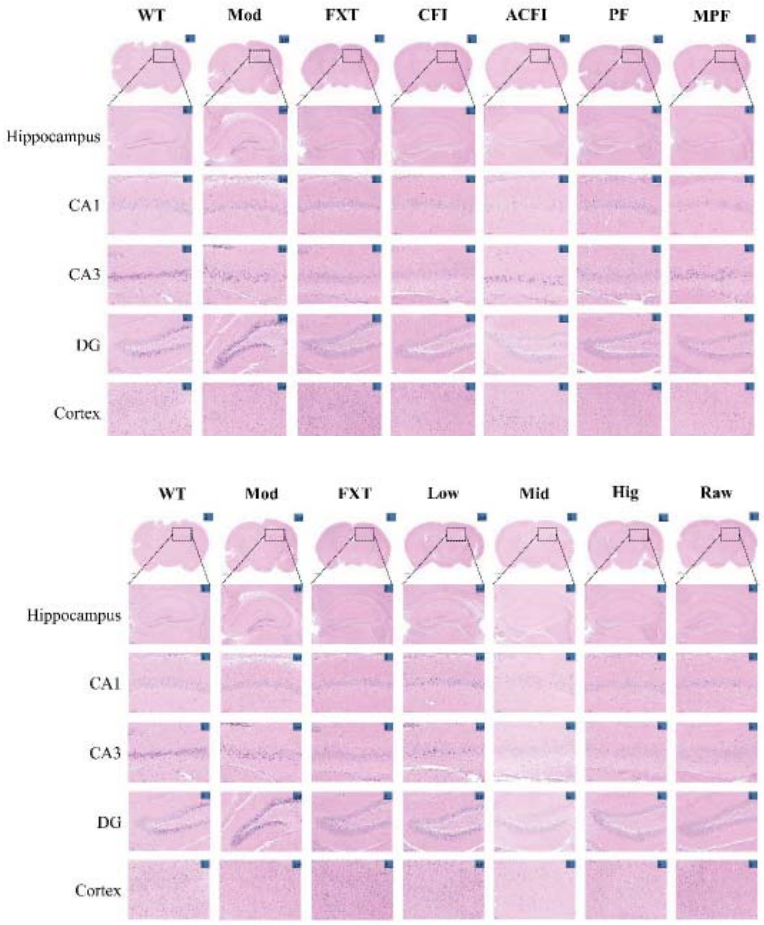

Figure 6 MZNNJ attenuates reserpine-induced neuronal damage in the hippocampus and cortex (H&E staining). Representative photomicrographs of (A) cortex and (B) hippocampal CA1, CA3, and DG regions. *n* = 3 mice per group were examined for histopathological evaluation.

enlarged synapses, and overall hippocampal atrophy. Compared to the Mod group, the CFI group showed no recovery in cortical neuron numbers, while hippocampal DG neurons recovered but without gap restoration. The ACFI group exhibited no significant recovery in cortical neurons but showed better recovery in hippocampal DG neurons. In the PF group, cortical neurons were disorganized with reduced numbers, and hippocampal DG neurons were disorganized without observed gap recovery. In the MPF group, cortical neurons were disorganized with reduced numbers, while hippocampal DG neuron numbers showed good recovery and gaps recovered well. In the MZNNJ Raw group, cortical neurons were disorganized with reduced numbers, hippocampal CA region cells were disorganized, and DG region showed recovery but retained disorganized cell arrangement. In the MZNNJ Low and Hig groups, cortical neuron numbers showed marked recovery. In the Low and mid groups, hippocampal CA region cell arrangement was disorganized, with marked recovery observed in the Low and Hig groups. In the FXT group, cortical neuron numbers showed significant recovery, with marked recovery in the DG region and no significant recovery in the CA region, as shown in figure 6A-B.

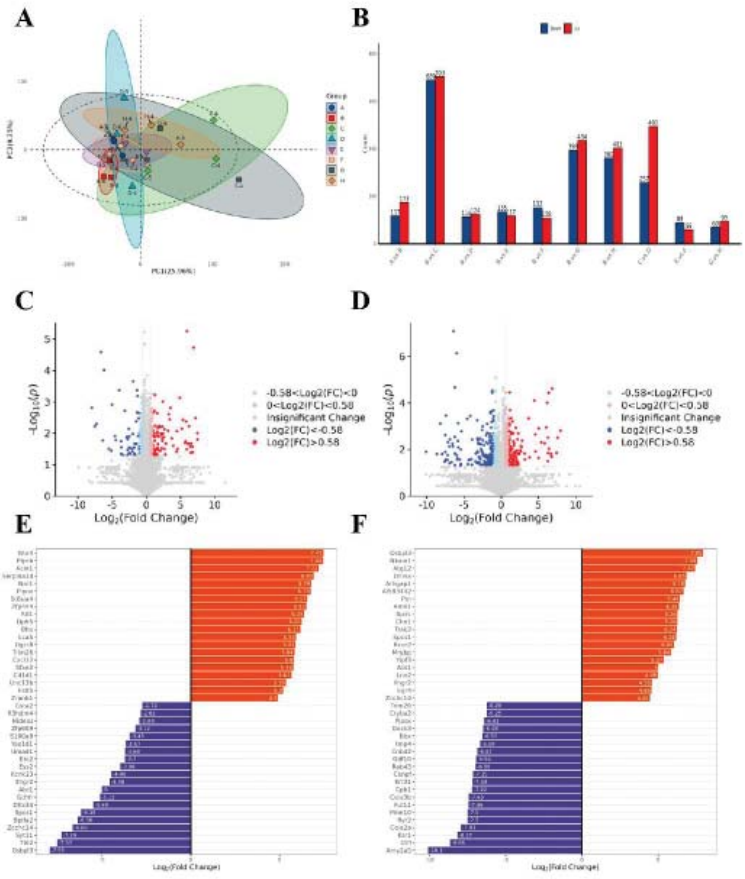

Figure 7 Proteomic profiling reveals differential protein expression in mouse brain tissue after MZNNJ treatment.

(A) Principal component analysis (PCA) score plot showing separation among per group. (B) Number of differentially expressed proteins (DEPs) identified in pairwise comparisons. (C) Volcano plot of DEPs between WT and Model groups. (D) Volcano plot of DEPs between Model and MZNNJ High-dose groups. (E) Bar chart of fold changes for the top 40 DEPs in WT vs. Model. (F) Bar chart of fold changes for the top 40 DEPs in Model vs. MZNNJ High-dose. DEPs were defined as |FC| ≥ 1.5 and $p < 0.05$. $n = 3$ biological replicates per group.

Proteomics analysis of mouse brain tissue

The PCA score plot in figure 7A shows that the Mod group (B) differs from the MZNNJ Hig group (H) along PC1 and from both the WT group (A) and MZNNJ Hig group (H) along PC2. PC1 and PC2 accounted for 25.96% and 9.35% of the protein variation among different groups, respectively. In the analysis of significantly different proteins, P-value and fold change (FC) were used as screening criteria to identify significantly altered proteins. The P-value threshold was set at <0.05, while the FC threshold was ≥1.5 or ≤1/1.5. Figure 7B shown the number of differentially expressed proteins (DEPs) identified in comparisons between different groups. Figure 7C-D volcano plots shows the DEPs in the WT-Mod group (A-B) and between the Mod-Hig group (B-H), with each dot representing a protein. Figure 7E-F displays bar charts of fold change for the top 40 DEPs in the WT-Mod group (A-B) and Mod-Hig group (B-H). These results provide a ground for further research on the functions of the DEPs.

Using Gene Ontology (GO) enrichment analysis, DEPs were divided into three categories: BP, CC, and MF. The results showed that the different proteins identified in WT-Mod group and Mod-Hig group were significantly enriched in the cell-cell signaling and synaptic signaling in BP, extracellular region and postsynapse in CC, and glutathione peroxidase activity and structural constituent of postsynapse in MF (Figure 8A-B). These results predict the function of differential protein enrichment. Figures 8C-F showes the relationship and chord diagrams between DEPs and pathways in the top 15 pathways for the WT-Mod and Mod-Hig groups, respectively, along with the top 30 Kyoto Encyclopedia of Genes and Genomes (KEGG) pathways with significant enrichment for these proteins. The differentially expressed proteins primarily participate in the nervous system, neurodegenerative diseases, signal transduction, and other processes. These differentially expressed proteins are mainly involved in immune and disease-related signaling pathways, playing crucial roles in relevant fie

Detection of signaling pathway proteins in mouse brain tissue

Following proteomic analysis, the Ras signaling pathway was selected as the significantly enriched pathway containing the differentially expressed protein Kinase Suppressor of Ras 1 (KSR1). As illustrated, Western Blot results revealed that compared to the WT group, the Mod group exhibited significantly reduced expression of KRS1, Ras, BDNF, p-ERK1/2, and p-CREB proteins. Conversely, expression levels of these five proteins significantly rebounded in the Low, Mid, Hig, and Raw groups. In the CFI, ACFI, PF, and MPF groups, these protein expressions were similarly significantly elevated, with the PF and MPF groups exhibiting particularly pronounced upregulation of KRS1, Ras, BDNF, and p-ERK1/2. Overall, target protein expression in the Mod group exhibited a consistent downregulation trend, whereas the Low/Mid/Hig/Raw and CFI/ACFI/PF/MPF groups reversed this downregulation, resulting in a significant restoration or elevation of protein expression levels (Figure 9).

Immunofluorescence detection of p-CREB protein

Immunofluorescence staining results for p-CREB in brain tissue revealed marked intergroup differences in red fluorescence intensity: the WT group maintained baseline red fluorescence for p-CREB, whereas the Mod group exhibited significantly diminished p-CREB fluorescence intensity, indicating successful model induction of CREB phosphorylation inhibition. Following intervention with the positive control drug FXT, p-CREB fluorescence

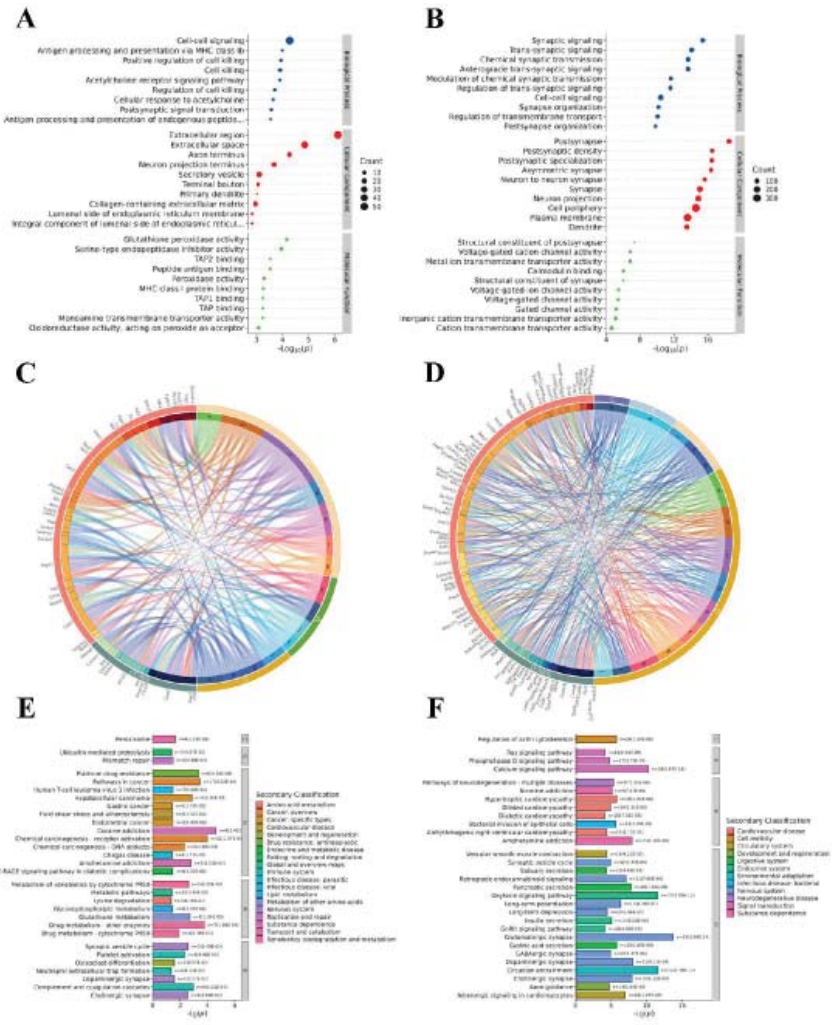

Figure 8 Functional enrichment analysis of differentially expressed proteins.

(A) GO enrichment analysis of DEPs in WT vs. Model group. (B) GO enrichment analysis of DEPs in Model vs. MZNNJ High-dose group. GO terms are categorized into biological process (BP), cellular component (CC), and molecular function (MF). (C) Chord diagram showing the relationship between DEPs and top 15 enriched pathways in WT vs. Model. (D) Chord diagram for Model vs. MZNNJ High-dose. (E) Top 30 KEGG pathways enriched in WT vs. Model. (F) Top 30 KEGG pathways enriched in Model vs. MZNNJ High-dose. The Ras signaling pathway and glutathione peroxidase activity were significantly enriched. *n* = 3 biological replicates per group.

intensity significantly recovered compared to the Mod group, with expression levels approaching those of the WT group. This confirms FXT's efficacy in restoring CREB phosphorylation activity. Across different intervention strategies, p-CREB fluorescence intensity in the Low, Mid, and Hig groups exhibited varying degrees of enhancement compared to the Mod group. The Mid and Hig groups demonstrated enhancement effects closer to those of the FXT group, whilst p-CREB expression in the Raw group showed no significant difference from the Mod group. The p-CREB fluorescence in the CFI, ACFI, PF, and MPF groups was elevated compared to the Mod group. The p-CREB recovery effect in the ACFI group was closer to that of the FXT group, while the enhancement in the PF and MPF groups was relatively moderate. These findings suggest that most treatment groups can reverse the model-induced inhibition of CREB phosphorylation to varying degrees, with some groups (e.g., Mid, Hig, ACFI) exhibiting regulatory effects

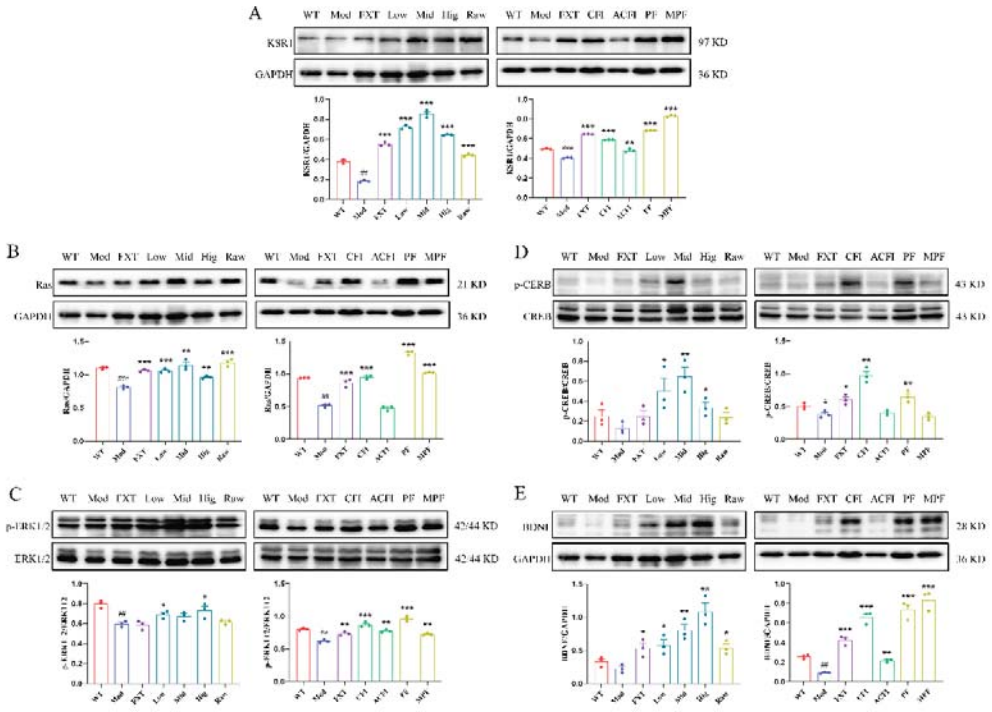

Figure 9 MZNNJ activates the KSR1/Ras/ERK/CREB/BDNF signaling pathway in mouse brain.

(A) Representative Western blot images of KSR1, Ras, p-ERK1/2, ERK1/2, p-CREB, CREB, and BDNF in brain tissue (upper panels) and quantitative analysis of protein expression (lower panels). (B) Ras, (C) p-ERK1/2/ERK1/2 ratio, (D) p-CREB/CREB ratio, (E) BDNF protein expression normalized to β-actin. Data are presented as mean ± SD (n = 3 per group). Statistical analysis was performed using one-way ANOVA followed by Tukey's post-hoc test for multiple comparisons. #$p < 0.05$, ##$p < 0.01$, ###$p < 0.001$ vs. WT group; *$p < 0.05$, **$p < 0.01$, ***$p < 0.001$ vs. Model group.

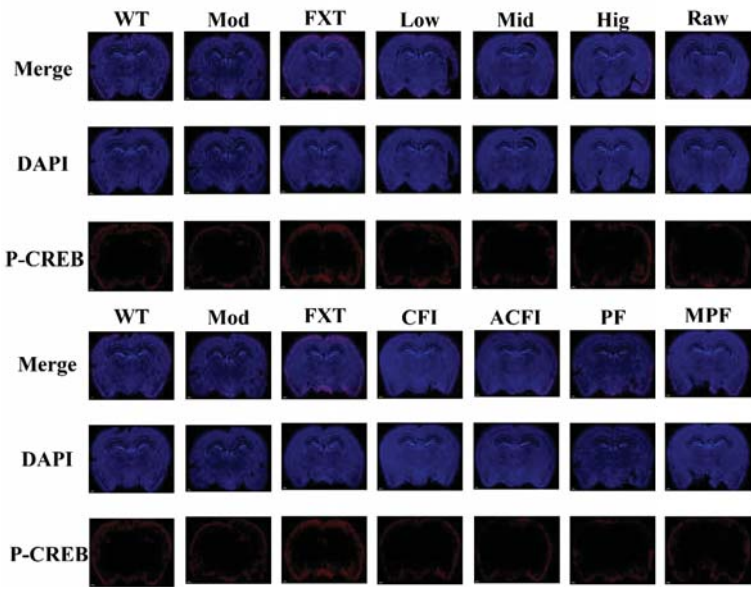

Figure 10 MZNNJ enhances p-CREB expression in mouse brain detected by immunofluorescence.

Representative immunofluorescence images of p-CREB (red) in brain sections. Nuclei were counterstained with DAPI (blue). *n* = 3 mice per group were examined for immunofluorescence staining.

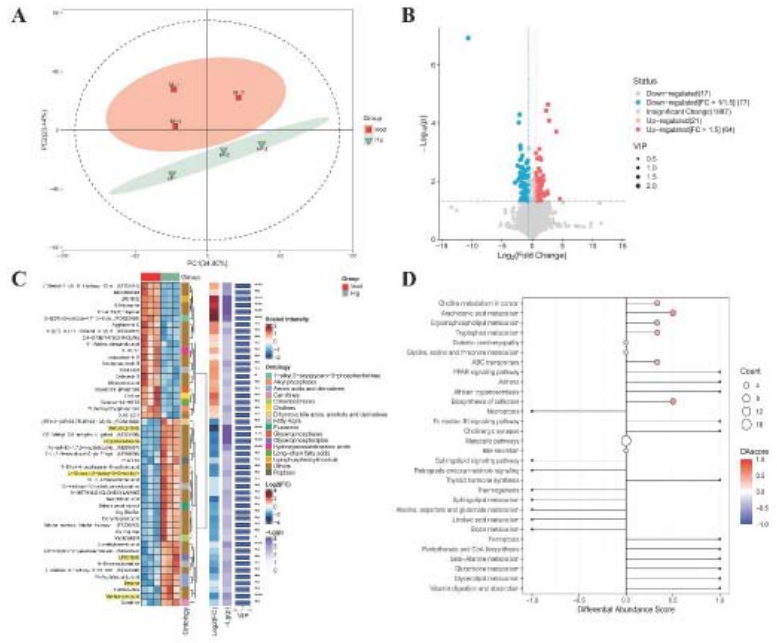

Figure 11 Serum metabolomics reveals MZNNJ-induced metabolic alterations.

(A) Principal component analysis (PCA) score plot showing distinct clustering between Mod group and MZNNJ-treated group in serum samples. (B) Volcano plot of differentially expressed metabolites in serum between Mod and MZNNJ-treated groups. (C) Heatmap of differentially expressed metabolites in serum. Each row represents a metabolite and each column represents a sample. Red indicates high expression and blue indicates low expression. (D) KEGG pathway enrichment analysis of differential serum metabolites. *n* = 6 biological replicates per group were analyzed by UHPLC-MS/MS.

comparable to the positive control FXT (Figure 10).

Metabolomics-based prediction of MZNNJ components entering the bloodstream and brain

Figure 11 demonstrates that for Group Mod vs. Group MZNNJ, the serum samples of the two groups exhibit distinct clustering separation in the PCA score plot. A total of 141 highly significant differential metabolites were identified, including 64 significantly upregulated metabolites and 77 significantly downregulated ones. In the heatmap of differential metabolites, components (e.g., vanilpyruvic acid, betaine, and cryptotanshinone) that are lowly expressed in Group Mod are all derived from different reactions (such as acetalization) of active ingredients (e.g., ellagic acid) in the Chinese medicinal materials of MZNNJ. These differential metabolites are mainly enriched in pathways including Choline metabolism in cancer and Glycerophospholipid metabolism, and also involve pathways related to neurotransmitter synthesis (e.g., sphingolipid metabolism and glutathione metabolism).

This indicates that, under the synergy of glycerophospholipid synthesis, neurotransmitter (acetylcholine) production, and methylation regulation, the pharmacodynamic components in MZNNJ take choline as the core link: they not only support the synthesis and homeostasis of membrane glycerophospholipids (phosphatidylcholine) but also participate in cholinergic neural signal transmission, while maintaining the balance of the cellular methyl donor pool via the betaine-methionine cycle.

In figure 12, for the Mod group vs. MZNNJ group, the brain tissue samples of the two groups showed distinct clustering separation in the PCA score plot. A total of 162 highly significant

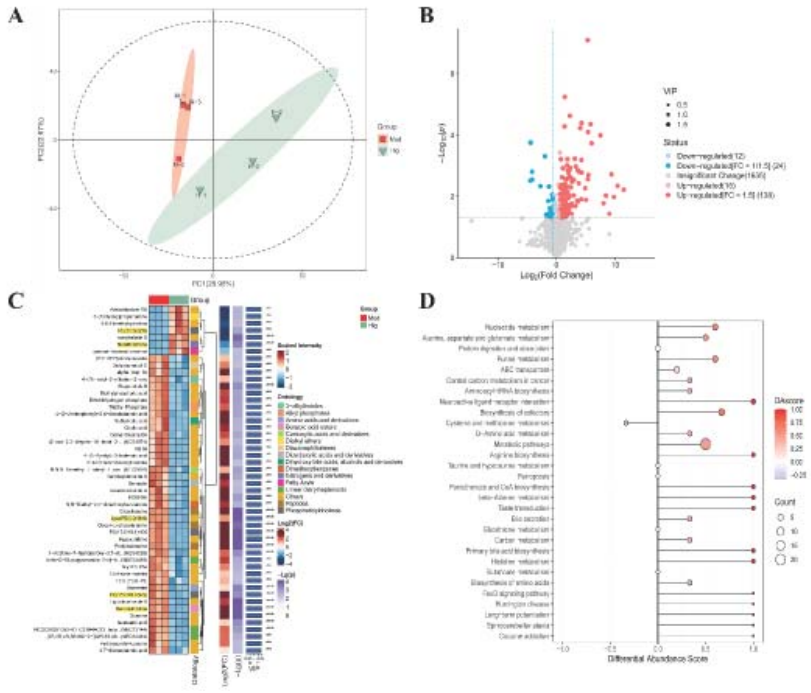

Figure 12 Brain metabolomics reveals MZNNJ-induced neuroprotective metabolic reprogramming.

(A) Principal component analysis (PCA) score plot showing distinct clustering between Mod group and MZNNJ-treated group in brain tissue samples. (B) Volcano plot of differentially expressed metabolites in brain tissue between Mod and MZNNJ-treated groups. (C) Heatmap of differentially expressed metabolites in brain tissue. Each row represents a metabolite and each column represents a sample. Red indicates high expression and blue indicates low expression. (D) KEGG pathway enrichment analysis of differential brain metabolites. *n* = 6 biological replicates per group were analyzed by UHPLC-MS/MS.

differential metabolites were identified, including 138 significantly upregulated metabolites and 24 significantly downregulated ones. These differential metabolites are mainly enriched in pathways such as Nucleotide metabolism, Alanine, aspartate and glutamate metabolism, Purine metabolism, and Spinocerebellar ataxia—most of which are associated with neurotoxic injury, excitatory metabolic disturbance, and apoptosis. Serving as core driver pathways in the central pathological process of depression, the excessive activation of these pathways may exacerbate the depressive phenotype by inducing neuronal damage and disrupting the homeostasis of neural circuits.

Additionally, other enriched pathways include Cysteine and methionine metabolism, Pantothenate and CoA biosynthesis, Glutathione metabolism, and Biosynthesis of amino acids, which possess functions such as antioxidative stress response, maintenance of energy metabolism homeostasis, regulation of cell survival, and improvement of synaptic plasticity. The suppressed activity of these pathways may lead to weakened central neuroprotective mechanisms, which is a key characteristic of metabolic disorders in the depressive model.

Discussion

In this study, we provide the first systematic demonstration that the classic Uyghur medicinal formula Maizhuni-Nujia (MZNNJ) exerts significant antidepressant-like effects in a reserpine-induced mouse model of acute depression. Our multi-dimensional approach revealed that MZNNJ's therapeutic action is not attributable to a single mechanism but rather arises from a sophisticated interplay of enhanced

neuroplasticity, systemic metabolic regulation, and optimized formulation chemistry grounded in traditional processing and compatibility principles.

MZNNJ ameliorates depressive-like behaviors by restoring monoamine and neurotrophic factor deficits

The reserpine model, which induces a rapid and profound depletion of monoamines, remains a relevant tool for probing mechanisms related to monoamine dysregulation and for the initial screening of potential antidepressants [11,14,18]. Our results confirm that reserpine administration successfully induced a robust depressive-like phenotype, characterized by significant behavioral despair (increased immobility/floating in the Morris water maze), motor retardation (ptosis, decreased swimming speed), and correspondingly low levels of 5-HT, DA, and BDNF [19,20]. MZNNJ treatment, particularly at medium and high doses, effectively reversed these deficits. The robust increase in both serum and brain DA and BDNF levels is particularly noteworthy. BDNF is a central mediator of neuroplasticity, promoting neuronal survival, synaptic growth, and long-term potentiation—processes critical for recovery from depression-related neural atrophy [5,21,22]. The correlation between elevated BDNF and improved behavioral outcomes supports MZNNJ's potential involvement in neuroplasticity enhancement, consistent with the widely accepted role of BDNF in antidepressant effects [21,24].

Activation of the KSR1/Ras/ERK/CREB/BDNF signaling axis: a novel upstream mechanism

The most innovative aspect of our finding is the specific upregulation of Kinase Suppressor of Ras 1 (KSR1). KSR1 is a scaffold protein that organizes signal transmission through the Raf/MEK/ERK kinase cascade, ensuring signaling efficiency and fidelity [29,30]. While KSR1 has been extensively studied in cancer biology, its role in the central nervous system remains largely unexplored [30,31]. Emerging evidence suggests that scaffold proteins are critical for the spatiotemporal regulation of synaptic signaling and are essential for forms of synaptic plasticity that require sustained ERK activation [32]. Our data demonstrate that MZNNJ upregulates KSR1, which correlates with enhanced phosphorylation of ERK and CREB—a pathway central to neuroplasticity [25-28]. This mechanism contrasts with conventional antidepressants that primarily target neurotransmitter transporters or receptors [6]. KSR1 thus represents a candidate for further investigation as a potential molecular node in antidepressant action.

The scientific basis of Uyghur processing and compatibility: from empirical art to molecular science

A unique and powerful aspect of our study was the comparative analysis between the Raw MZNNJ formulation (containing unprocessed CFI and PF) and the processed formulation (containing ACFI and MPF). The markedly superior efficacy of the processed formulation across behavioral, neurochemical, and molecular endpoints provides direct experimental validation for the traditional practices of "paozhi" (processing) [9,10].

Our data suggest that processing with milk (for PF) and apricot kernel oil (for CFI) is not merely a ritualistic step but serves to optimize the biopharmaceutical properties and enhance the therapeutic potential of the herbs. Modern research supports this view, demonstrating that processing can significantly enhance efficacy through chemical transformations, such as glycoside hydrolysis, which generate more bioavailable compounds, and through the use of adjuvants that facilitate the dissolution, absorption, and targeted distribution of active

components [33-35]. The particularly potent activation of the KSR1/Ras/ERK/CREB/BDNF pathway by ACFI and MPF, both as single entities and within the full formula, indicates that processing likely enriches or transforms the constituents responsible for targeting this critical pathway. This finding provides a modern molecular rationale for the traditional emphasis on processing.

Furthermore, the superior performance of the full processed formula compared to any single herb or simple combination highlights the wisdom of the "Jun-Chen-Zuo-Shi" (sovereign-minister-assistant-courier) compatibility principle [36,37]. Our data suggests a functional division of labor within the formula. The processed sovereign herbs (ACFI and MPF) act as the primary drivers of neurotrophic signaling (the "engine"). The minister and assistant herbs (Cuscuta, Lavandula, Polypodiode) may contribute by modulating other relevant systems, such as providing antioxidant support, dampening neuroinflammation, or fine-tuning monoamine levels, thereby creating a supportive "chassis" for the engine's action [38]. The honey base, beyond its role as a binder, may facilitate absorption and harmonize the actions of the different components [39]. The superior performance of the full processed formula supports a multi-target, synergistic action, which may offer advantages over single-target agents for treating depression [37,40].

Metabolomics reveals systemic regulation of neuroprotection and energy metabolism

Our untargeted metabolomics analysis provides a novel and comprehensive perspective on MZNNJ's mechanism, placing it within the broader context of brain metabolic homeostasis. Depression is increasingly viewed not just as a disorder of neurotransmission, but as a systemic metabolic disorder involving impaired cerebral energy metabolism, mitochondrial dysfunction, and oxidative stress [41,42].

The enrichment of pathways related to glutathione metabolism is of particular significance. Glutathione (GSH) is the brain's primary endogenous antioxidant, crucial for neutralizing Reactive Oxygen Species (ROS) and maintaining the redox balance [43]. Oxidative stress is a well-documented feature of depression, contributing to neuronal damage and neuroinflammation [44]. Furthermore, oxidative stress and lipid peroxidation are central drivers of ferroptosis, a recently characterized form of regulated cell death that has been strongly implicated in the pathophysiology of depression [45,46]. By modulating GSH metabolism, MZNNJ may be bolstering the brain's antioxidant defenses, thereby protecting neurons from oxidative damage and potentially inhibiting ferroptosis processes, as suggested by a recent breakthrough showing that metabolites like itaconate can directly protect against ferroptosis by modifying glutathione peroxidase 4 (GPx4) [47].

The enrichment of the "Spinocerebellar ataxia" pathway is a particularly intriguing and profound finding. While this pathway is classically associated with a specific neurodegenerative disease, its core components involve glutamate-mediated excitotoxicity, mitochondrial dysfunction, and disruptions in calcium homeostasis—all of which are increasingly recognized as key pathological drivers in depression as well [48,49]. This overlap suggests that MZNNJ's effects may extend to mitigating excitotoxic damage and stabilizing neuronal firing. Moreover, the regulation of energy metabolism pathways (e.g., alanine, aspartate and glutamate metabolism) indicates that MZNNJ can address the cerebral energy deficit characteristic of the depressed brain [50]. By improving the brain's energy status and reducing excitotoxicity, MZNNJ may create a more favorable metabolic microenvironment that supports neuron-glia metabolic coupling and allows for the synaptic remodeling driven

by the activation of the BDNF pathway [51]. This dual action—promoting intrinsic repair pathways while correcting the adverse metabolic milieu—highlights a promising therapeutic strategy for depression [41,42].

Limitations regarding mechanistic interpretation

While the present study provides comprehensive and multi-layered evidence linking MZNNJ treatment to KSR1 upregulation and activation of the Ras/ERK/CREB/BDNF signaling pathway, it is important to acknowledge that these findings are primarily correlational in nature. The proteomic, Western blotting, and immunofluorescence data robustly demonstrate strong associations between MZNNJ administration, increased KSR1 expression, enhanced phosphorylation of ERK and CREB, elevated BDNF levels, and amelioration of depressive-like behaviors. However, these observations do not, by themselves, establish a direct causal relationship between KSR1 pathway activation and the antidepressant effects of MZNNJ.

Several factors constrain the definitive interpretation of our mechanistic data. First, the proteomic analysis was conducted on whole-brain tissue homogenates, which cannot distinguish cell-type-specific changes or capture the spatial and temporal dynamics of pathway activation within distinct neural circuits. KSR1 is known to function as a scaffolding protein that organizes the Raf/MEK/ERK cascade in a compartment-specific manner within hippocampal neurons, and its subcellular localization is critical for the spatiotemporal regulation of ERK signaling during synaptic plasticity. Whole-tissue analysis thus masks these potentially important regional and subcellular differences. Second, while the concurrent upregulation of KSR1 and downstream pathway components is highly suggestive, it remains possible that MZNNJ exerts its antidepressant effects through parallel or intersecting pathways that are independent of KSR1, such as the PI3K/AKT/mTOR axis or neuroinflammatory pathways, which were not fully explored in the current study. Third, the reserpine model itself induces acute monoamine depletion, which may trigger distinct molecular responses compared to the chronic, multifactorial pathophysiology of human major depressive disorder. Unlike chronic unpredictable mild stress models that better recapitulate the progressive and multifaceted nature of depression, the reserpine model primarily reflects acute pharmacological disruption of monoamine storage.

To definitively establish causality, future studies employing loss-of-function approaches—such as siRNA-mediated knockdown or conditional knockout of KSR1 in specific brain regions (e.g., hippocampus or prefrontal cortex)—are warranted. Additionally, pharmacological inhibition of downstream nodes (e.g., using MEK inhibitors such as PD0325901) would help determine whether the behavioral and neurochemical effects of MZNNJ are indeed mediated through this pathway. Complementary approaches, including viral-mediated overexpression of KSR1 or BDNF in the absence of MZNNJ treatment, could further elucidate whether KSR1 activation alone is sufficient to recapitulate the observed antidepressant-like effects. These strategies will be essential to confirm the causal role of the KSR1/Ras/ERK/CREB/BDNF cascade in mediating the therapeutic actions of MZNNJ. Until such experiments are performed, our conclusions regarding the mechanistic involvement of this pathway should be interpreted with appropriate caution, and our discussion has been framed accordingly.

While our study provides robust and multi-faceted evidence for the antidepressant effects and mechanisms of MZNNJ, several limitations should be acknowledged. First, the reserpine-

induced acute depression model, while valuable for studying monoamine depletion [11,13,14], does not fully recapitulate the chronic, complex, and progressive nature of human MDD. Reserpine induces rapid depletion of monoamines via irreversible inhibition of VMAT2, leading to acute behavioral changes that are largely reversible. In contrast, human MDD typically involves complex interactions among genetic susceptibility, chronic stress, neuroinflammation, and impaired neuroplasticity—factors not adequately modeled by acute reserpine administration. Furthermore, the acute nature of this model does not capture the disease chronicity and recurrent episodes characteristic of clinical depression. Future studies using more translationally relevant models, such as chronic unpredictable mild stress (CUMS) or social defeat stress models, are necessary to validate the long-term efficacy and neuroplasticity-promoting effects of MZNNJ [52]. Second, although we identified the activation of the KSR1/Ras/ERK/CREB/BDNF pathway, the precise molecular events are correlational. The specific bioactive compounds within MZNNJ responsible for this activation, and their direct molecular targets (e.g., upstream receptors like TrkB), need to be identified through techniques such as affinity purification, molecular docking, and cellular thermal shift assays [53]. Third, the metabolomic findings, while highly suggestive, require further validation through targeted metabolomics and functional assays to confirm the impact on specific metabolic fluxes, such as GSH synthesis or mitochondrial respiration [43]. Finally, the use of a single species (mice) and the absence of separate sex-specific subgroup analyses limit the generalizability of our findings; further studies with larger sample sizes and sex-specific analyses are warranted. These considerations underscore the importance of interpreting our results as a foundational step toward understanding MZNNJ's therapeutic potential, rather than as definitive clinical validation.

Conclusions

In conclusion, this study provides the first comprehensive evidence that Maizhuni-Nujia (MZNNJ), a classic Uyghur medicinal formula, exerts potent antidepressant-like effects in a reserpine-induced mouse model of depression. Its therapeutic superiority is rooted in the synergistic interplay of its processed constituents, validating the scientific basis of traditional Uyghur processing and compatibility principles. Mechanistically, MZNNJ acts through a novel, multi-tiered strategy: it potently activates the KSR1-mediated Ras/ERK/CREB/BDNF neurotrophic signaling pathway to promote neuroplasticity and neuronal repair, while simultaneously correcting brain metabolic disturbances related to antioxidant defense (glutathione metabolism), energy production, and excitotoxicity. This positions MZNNJ not merely as a monoamine modulator, but as a systemic regulator of brain health. By linking a traditional processing technique to the modulation of a key upstream scaffold protein (KSR1), our findings open a new avenue for antidepressant drug discovery. This work provides a robust modern pharmacological foundation for the clinical application of MZNNJ and establishes a paradigm for the scientific investigation of complex ethnomedical formulations.

Author Contributions

Gvlzapar Tohniyaz: Conceptualization, Methodology, Investigation, Data Curation, Writing-original draft, Funding acquisition. Wei Chen: Investigation, Validation, Resources, Funding acquisition. Zhe Xu: Methodology. Yanchuan Gong: Investigation. Qin Ma: Supervision, Project administration, Funding acquisition.

Institutional Review Board Statement

The animal study protocol was approved by the

Animal Ethics Committee of the Xinjiang Corps Key Laboratory of Bone Health and Traditional Chinese Medicine Research (Approval number: HSD-20241110-04).

Informed Consent Statement

Not applicable. This study does not involve human subjects, human tissue, or personal data.

Data Availability Statement

The data presented in this study are available on request from the corresponding author.

Conflicts of Interest

The authors declare that they have no known competing financial interests or personal relationships that could have appeared to influence the work reported in this paper.

Funding information

This research was funded by the Xinjiang Tianshan talented youth top talent project (Chen Wei, 2022TSYCCY0014), Xinjiang Uygur Autonomous Region Natural Science Foundation (2023D01F31), Xinjiang Uygur Autonomous Region Key Science and Technology R&D Projects (2022B03007-3) and the Science and Technology Programme Projects of the Xinjiang Production and Construction Corps (2023AB044).

References

1. Hasler G. Pathophysiology of depression: do we have any solid evidence of interest to clinicians? World Psychiatry. 2010;9(3):155-61. doi:10.1002/j.2051-5545.2010.tb00298.x.
2. Pitsillou E, Bresnehan SM, Kagarakis EA, Wijoyo SJ, Liang J, Hung A, et al. The cellular and molecular basis of major depressive disorder: towards a unified model for understanding clinical depression. Mol Biol Rep. 2020;47(1):753-70. doi:10.1007/s11033-019-05129-3.
3. Marsden WN. Synaptic plasticity in depression: molecular, cellular and functional correlates. Prog Neuropsychopharmacol Biol Psychiatry. 2013;43:168-84. doi:10.1016/j.pnpbp.2012.12.012.
4. Walker ER, McGee RE, Druss BG. Mortality in mental disorders and global disease burden implications. JAMA Psychiatry. 2015;72(4):334-41. doi:10.1001/jamapsychiatry.2014.2502.
5. Duman RS, Deyama S, Fogaça MV. Role of BDNF in the pathophysiology and treatment of depression: activity-dependent effects distinguish rapid-acting antidepressants. Eur J Neurosci. 2021;53(1):126-39. doi:10.1111/ejn.14630.
6. Jiang Y, Zhang L, Rui Y, Li J, Xu Y, Zhu X, et al. Monoamine neurotransmitters control basic emotions and affect major depressive disorders. Pharmaceuticals (Basel). 2022;15(10):1203. doi:10.3390/ph15101203.
7. German-Ponciano LJ, Rosas-Sánchez GU, Rivadeneyra-Domínguez E, Rodríguez-Landa JF. Participation of the serotonergic system and brain-derived neurotrophic factor in the antidepressant-like effect of flavonoids. Int J Mol Sci. 2022;23(18):10881. doi:10.3390/ijms231810881.
8. Xu Y, Zhang Y, Li X, Wang Y, Liu J, Chen L, et al. Engeletin alleviates depression-like phenotype by increasing synaptic plasticity via the BDNF-TrkB-mTORC1 signalling pathway. J Cell Mol Med. 2023;27(23):3928-38. doi:10.1111/jcmm.18011.
9. Wang YZ, Zhang H, Li X, Zhao Y, Liu Y, Chen J, et al. Discussion on the effects of Chinese medicine processing on the changes of medicinal properties based on the changes of chemical constituents and pharmacodynamic perspective. J Ethnopharmacol. 2025;346:119122.
10. Zhao Z, Liang Z, Chan K, Lu G, Lee EL, Chen H, et al. A unique issue in the standardization of Chinese materia medica: processing. Planta Med. 2010;76(17):1975-86. doi:10.1055/s-0030-1250512.
11. Baumeister AA, Hawkins MF, Uzelac SM. The myth of reserpine-induced depression: role in the historical development of the monoamine hypothesis. J Hist Neurosci. 2003;12(2):207-20. doi:10.1076/jhin.12.2.207.15535.
12. Telega LM, Wróbel A, Gawliński D, Korga A, Sypecka J, Rog J, et al. Reserpine-induced rat model for depression: behavioral, physiological and PET-based dopamine receptor availability validation. Prog Neuropsychopharmacol Biol Psychiatry. 2024;133:110987.
13. Mulinari S. Monoamine theories of depression:

historical impact on biomedical research. J Hist Neurosci. 2012;21(4):366-92. doi:10.1080/0964704X.2011.623917.

14. Antkiewicz-Michaluk L, Romańska I, Michaluk J, Vetulani J. Withdrawal from repeated administration of a low dose of reserpine induced opposing adaptive changes in the noradrenaline and serotonin system function: a behavioral and neurochemical ex vivo and in vivo study in the rat. Prog Neuropsychopharmacol Biol Psychiatry. 2015;57:146-54. doi:10.1016/j.pnpbp.2014.11.006.

15. de Freitas CM, Busanello A, Schaffer LF, Kaster MP, Ardais AP, Moretti M, et al. Behavioral and neurochemical effects induced by reserpine in mice. Psychopharmacology (Berl). 2016;233(3):457-67. doi:10.1007/s00213-015-4137-7.

16. Vorhees CV, Williams MT. Morris water maze: procedures for assessing spatial and related forms of learning and memory. Nat Protoc. 2006;1(2):848-58. doi:10.1038/nprot.2006.116.

17. Parrini M, Caroni P, Spolidoro M. Protocol to investigate the gradual selection and deployment of goal-oriented search strategies during unsupervised navigation in mice. STAR Protoc. 2024;5(3):103305. doi:10.1016/j.xpro.2024.103305.

18. Leão AHFF, Guzen FP, de Oliveira KC, Araújo NB, de Sousa RT, Cavalcante JS, et al. Changes in the mesocorticolimbic pathway after low-dose reserpine treatment in Wistar and spontaneously hypertensive rats (SHR): Implications for cognitive deficits in a progressive animal model for Parkinson's disease. Behav Brain Res. 2021;410:113349. doi:10.1016/j.bbr.2021.113349.

19. Maácz F, Horti F, Csorba A, Tóth A, Mike A, Sperlágh B. The role of the vesicular monoamine transporter 2 in the inhibitory effect of tetrabenazine and valbenazine compared to reserpine on the vesicular release of monoamine transmitters. Front Cell Neurosci. 2025;19:1581855. doi:10.3389/fncel.2025.1581855.

20. Mohammed HS, El-Hawary SS, Abd El-Aziz NM, Hassan HM, Abdel-Hamid NM, Abdelrahman RS, et al. Assessment of the therapeutic potential of hesperidin and quercetin nanoparticles on oxidative stress, enzyme activities, trophic factors, and monoamines in an animal model of depression. Neurochem Res. 2025;50(4):1547-66. doi:10.1007/s11064-025-04477-2.

21. Björkholm C, Monteggia LM. BDNF: a key transducer of antidepressant effects. Neuropharmacology. 2016;102:72-9. doi:10.1016/j.neuropharm.2015.10.034.

22. Tartt AN, Mariani MB, Hen R, Mann JJ, Boldrini M. Dysregulation of adult hippocampal neuroplasticity in major depression: pathogenesis and therapeutic implications. Mol Psychiatry. 2022;27(6):2689-709. doi:10.1038/s41380-022-01520-x.

23. Pardossi S, Fagiolini A, Cuomo A. Variations in BDNF and their role in the neurotrophic antidepressant mechanisms of ketamine and esketamine: a review. Int J Mol Sci. 2024;25(23):12769. doi:10.3390/ijms252312769.

24. Cavaleri D, Riboldi I, Daccò S, Cattaneo A, Poletti S, Benedetti F, et al. The role of BDNF in major depressive disorder, related clinical features, and antidepressant treatment: insight from meta-analyses. Neurosci Biobehav Rev. 2023;149:105173. doi:10.1016/j.neubiorev.2023.105173.

25. Li SY, Li XX, Zhang Y, Wang Y, Liu Z, Wang LP. Auricular electroacupuncture improves depression possibly by promoting hippocampal Raf/ERK/RSK/CREB signaling in chronic unpredictable mild stress-induced depression rats. Zhen Ci Yan Jiu. 2019;44(8):554-9. Chinese.

26. Li X, Wang LP, Zhang Y, Liu Z, Li SY, Zhao Y. Effect of acupuncture intervention on depression behavior and expression of ERK1/2 and BDNF in prefrontal cortex in chronic unpredictable mild stress-induced depression rats. Zhen Ci Yan Jiu. 2018;43(11):705-10. Chinese.

27. Han X, Yang J, Song Y, Yang J, Chen L, Wang Y, et al. The mechanism of electroacupuncture for depression on basic research: a systematic review. Chin Med (Lond). 2021;16(1):10. doi:10.1186/s13020-020-00427-9.

28. Holderbach R, Clark K, Moreau JL, Bischofberger J, Normann C. Enhanced long-term synaptic depression in an animal model of depression. Biol Psychiatry. 2007;62(1):92-100. doi:10.1016/j.biopsych.2006.09.047.

29. Moon H, Kim JH, Lee SH, Park J, Kim Y, Lee J, et al. Targeting kinase suppressor of Ras 1 (KSR1) for cancer therapy. Pharmaceutics. 2025;17(10):1387. doi:10.3390/pharmaceutics17101387.

30. Bahar ME, Kim HJ, Kim DR. Targeting the RAS/RAF/MAPK pathway for cancer therapy: from mechanism to clinical studies. Signal Transduct Target Ther. 2023;8(1):361. doi:10.1038/s41392-023-01623-8.

31. Zhang S, Wang X, Li Y, Chen Z, Liu Y, Zhang L, et al. Tumor initiation and early tumorigenesis: molecular mechanisms and interventional targets. Signal Transduct Target Ther. 2024;9(1):96. doi:10.1038/s41392-024-01831-2.

32. Sweatt JD. The neuronal MAP kinase cascade: a biochemical signal integration system subserving synaptic plasticity and memory. J

Neurochem. 2001;76(1):1-10. doi:10.1046/j.1471-4159.2001.00054.x.

33. Deyama S, Duman RS. Neurotrophic mechanisms underlying the rapid and sustained antidepressant actions of ketamine. Pharmacol Biochem Behav. 2020;188:172837. doi:10.1016/j.pbb.2019.172837.

34. Yang B, Wang Y, Li H, Zhang Y, Zhao X, Liu J, et al. Interpreting the efficacy enhancement mechanism of Chinese medicine processing from a biopharmaceutic perspective. Chin Med (Lond). 2024;19(1):29. doi:10.1186/s13020-024-00895-4.

35. Shan Q, Wang H, Li Y, Zhang J, Liu X, Zhao Z, et al. Detoxification and underlying mechanisms towards toxic alkaloids by traditional Chinese medicine processing: a comprehensive review. Phytomedicine. 2024;129:155611. doi:10.1016/j.phymed.2024.155611.

36. Wang S, Hu Y, Tan W, Wu X, Chen R, Cao J, et al. Compatibility art of traditional Chinese medicine: from the perspective of herb pairs. J Ethnopharmacol. 2012;143(2):412-23. doi:10.1016/j.jep.2012.07.033.

37. Zhou X, Seto SW, Chang D, Kiat H, Razmovski-Naumovski V, Chan K, et al. Synergistic effects of Chinese herbal medicine: a comprehensive review of methodology and current research. Front Pharmacol. 2016;7:201. doi:10.3389/fphar.2016.00201.

38. Zhang W, Tao Q, Guo Z, Fu Y, Chen X, Shar PA, et al. Systems pharmacology for investigation of the mechanisms of action of traditional Chinese medicine in drug discovery. Front Pharmacol. 2019;10:743. doi:10.3389/fphar.2019.00743.

39. Ediriweera ERHS, Premarathna NYS. Medicinal and cosmetic uses of bee's honey: a review. AYU. 2012;33(2):178-82. doi:10.4103/0974-8520.105233.

40. Hopkins AL. Network pharmacology: the next paradigm in drug discovery. Nat Chem Biol. 2008;4(11):682-90. doi:10.1038/nchembio.118.

41. Liu X, Zhang Y, Chen L, Wang H, Li J, Zhao Y, et al. The ferroptosis-mitochondrial axis in depression: unraveling the feedforward loop of oxidative stress, metabolic homeostasis dysregulation, and neuroinflammation. Antioxidants (Basel). 2025;14(5):582. doi:10.3390/antiox14050582.

42. Zuo C, Huang Y, Bajis R, Sah VK, Li Y, Zhang G, et al. Nrf2: an all-rounder in depression. Redox Biol. 2022;58:102523. doi:10.1016/j.redox.2022.102523.

43. Dringen R. Metabolism and functions of glutathione in brain. Prog Neurobiol. 2000;62(6):649-71. doi:10.1016/S0301-0082(99)00060-X.

44. Maes M, Kubera M, Obuchowiczwa E, Goehler L, Brzeszcz J. A review on the oxidative and nitrosative stress (O&NS) pathways in major depression and their possible contribution to the (neuro)degenerative processes in that illness. Prog Neuropsychopharmacol Biol Psychiatry. 2011;35(3):676-92. doi:10.1016/j.pnpbp.2010.05.004.

45. Li E, Wang Y, Zhang X, Liu J, Zhao H, Chen L, et al. Inhibition of ferroptosis alleviates chronic unpredictable mild stress-induced depression in mice via tsRNA-3029b. Brain Res Bull. 2023;204:110831. doi:10.1016/j.brainresbull.2023.110831.

46. Cao H, Wang L, Sun X, Zhang Y, Liu J, Li H, et al. Hippocampal proteomic analysis reveals activation of necroptosis and ferroptosis in a mouse model of chronic unpredictable mild stress-induced depression. Behav Brain Res. 2021;407:113261. doi:10.1016/j.bbr.2021.113261.

47. Wei C, Zhang Y, Liu X, Li Y, Wang H, Chen L, et al. Itaconate protects ferroptotic neurons by alkylating GPx4 post stroke. Cell Death Differ. 2024;31(8):983-98. doi:10.1038/s41418-024-01308-8.

48. Sanacora G, Treccani G, Popoli M. Towards a glutamate hypothesis of depression. Neuropharmacology. 2012;62(1):63-77. doi:10.1016/j.neuropharm.2011.07.036.

49. Mattson MP. Glutamate and neurotrophic factors in neuronal plasticity and disease. Ann N Y Acad Sci. 2008;1144:97-112. doi:10.1196/annals.1418.005.

50. Gardner A, Boles RG. Is a "mitochondrial psychiatry" in the future? A review. Curr Psychiatry Rev. 2005;1(3):255-71.

51. Magistretti PJ, Allaman I. Lactate in the brain: from metabolic end-product to signalling molecule. Nat Rev Neurosci. 2018;19(4):235-49. doi:10.1038/nrn.2018.19.

52. Willner P. The chronic mild stress (CMS) model of depression: history, evaluation and usage. Neurobiol Stress. 2017;6:78-93. doi:10.1016/j.ynstr.2016.08.002.

53. Brunello CA, Cannarozzo C, Castrén E. Rethinking the role of TRKB in the action of antidepressants and psychedelics. Trends Neurosci. 2024;47(11):865-74. doi:10.1016/j.tins.2024.08.003.